Nano Research
2023, 16(6): 8405–8410
ISSN 1998-0124 CN 11-5974/O4
https://doi.org/10.1007/s12274-022-5300-8

Research Article

Designing a photo-assisted Co-C_3N_4 cathode for high performance Li-O_2 batteries

Renfei Cao[1,2], Yangfeng Cui[1,2], Gang Huang[2], Wanqiang Liu[1] (✉), Jianwei Liu[1,2] (✉), and Xinbo Zhang[2] (✉)

[1] School of Materials Science and Engineering, Changchun University of Science and Technology, Changchun 130022, China
[2] State Key Laboratory of Rare Earth Resource Utilization, Changchun Institute of Applied Chemistry, Chinese Academy of Sciences, Changchun 130022, China

Received: 18 September 2022 / **Revised:** 2 November 2022 / **Accepted:** 6 November 2022

ABSTRACT

Li-O_2 batteries with extremely high specific energy density have been regarded as a kind of promising successor to current Li-ion batteries. However, the high charge overpotential for the decomposition of Li_2O_2 discharge product reduces the energy efficiency and triggers a series of side reactions that cause the Li-O_2 batteries to have a limited lifetime. Herein, Co-doped C_3N_4 (Co-C_3N_4) photocatalysts were designed by an *in situ* thermal evaporation method to take advantage of the photo-assisted charging technology to conquer the shortcomings of Li-O_2 batteries encountered in the charge process. Different from the commonly used photocatalysts, the Co-C_3N_4 photocatalysts perform well no matter with and without illumination, owing to the Co doping induced conductivity and electrocatalytic ability enhancement. This makes the Co-C_3N_4 reduce the charge and discharge overpotentials and improve the cycling performance of Li-O_2 batteries (from 20 to 106 cycles) without illumination. While introducing illumination, the performance can be further improved: Charge voltage reduces to 3.3 V, and the energy efficiency increases to 84.84%, indicating that the Co-C_3N_4 could behave as a suitable photocathode for Li-O_2 batteries. Besides, the low charge voltage and the continuous illumination together weaken the corrosion of the Li anode, making the long-term high-efficiency operation of Li-O_2 batteries no longer just extravagant hope.

KEYWORDS

low overpotential, photocatalysis, lithium peroxide, Co-doped C_3N_4 (Co-C_3N_4), Li-O_2 batteries

1 Introduction

Non-aqueous Li-O_2 batteries have shown great competitiveness in available battery systems due to their ultra-high theoretical specific capacity (≈ 3,500 Wh·kg^{-1}), hoping to replace Li-ion batteries as the next generation of power batteries for electric vehicles[1–5]. Compared with the rocking-chair reaction model of Li-ion batteries, Li-O_2 batteries are based on the reversible formation and decomposition of Li_2O_2 ($2Li + O_2 \leftrightarrow Li_2O_2$), in which lithium metal as the anode, and oxygen as the cathode active substance with the Li_2O_2 discharge products grown on the porous cathode [6–8]. Despite promising, the insoluble and insulating nature of Li_2O_2 makes it high-efficiency decomposition is really a tough task, leading to a high charge overpotential that would continuously cause a series of side reactions and accordingly deteriorate the battery performance [9, 10]. To lower the charge overpotential, introducing solid catalysts or soluble redox mediators (RMs) has been shown to have some effect [11–14]. Among them, noble metal-based electrocatalysts such as Ru, Ir, and Au are considered to be excellent solid catalysts to reduce the polarization of oxygen evolution reaction (OER)[15–19]. However, most of them are only effective at the initial stage of charge, and the charge potential shows an increasing trend as the increase of charge depth, which usually reaches 4 V or higher, making the long-term running of Li-O_2 batteries full of thorns [6]. While for adding RMs into the electrolytes as soluble catalysts, they can facilitate the decomposition of Li_2O_2 and some by-products at their own oxidation potentials, providing flat charge profiles at low overpotentials and thus prolonging the lifetime of batteries [20, 21]. Although effective, the mobile nature of RMs could corrode the Li anode, and their stability toward the oxidative intermediates of Li-O_2 batteries is still a question [22, 23], rendering them to lose their functions in long-time cycling. Therefore, it is necessary to solve the shortcomings of prior art and propose a strategy to reduce the overpotential that could sustain a long time.

Recently, clean energy becomes the focus of research as the goal of carbon neutrality has been proposed [24]. To this end, the sustainable and green solar energy has received extensive attention in the field of energy conversion and storage [25, 26]. If Li-O_2 batteries integrate with a well-designed photocatalyst in the cathode side, it has a possibility to reduce the charge overpotential while using solar energy to charge. Wu et al. took the lead in verifying the feasibility of this kind of photo-assisted charge to decompose the Li_2O_2 discharge product at a low charge overpotential due to the photo-generated voltage [27]. Subsequently, different photoelectric materials, like C_3N_4 and TiO_2, were developed as the cathodes for Li-O_2 batteries to promote the low-overpotential decomposition of Li_2O_2 and consequently alleviate the high charge voltage induced side reactions [16, 28, 29]. Although the results are exciting,

Address correspondence to Wanqiang Liu, wqliu1979@126.com; Jianwei Liu, snowlover@ciac.ac.cn; Xinbo Zhang, xbzhang@ciac.ac.cn

unfortunately, the poor electrical conductivity of the reported semiconductor photocatalysts limits their ability to be fully functioned, leading to finite performance improvement for Li-O_2 batteries, and also the internal mechanism of the photo-assisted low charge overpotential is not yet clear.

Inspired by these challenges, we have designed a new photo-responsive cathode by in site growing Co-doped C_3N_4 (Co-C_3N_4) on the carbon paper (CP). The Co doping can not only improve the electrical conductivity and electrocatalytic ability, but also regulate the band gap to broaden the optical response wavelength range and enhance the photocatalytic property of C_3N_4. As a result, the Co-C_3N_4 reduces the charge potential from 3.90 to 3.30 V with an energy efficiency reaching 84.84% under simulated sunlight and enables the Li-O_2 battery to be stably cycled over 300 h at a charge voltage below 3.5 V. Even without illumination, the Co-C_3N_4 could still lower the polarization potential and improves the cycle life of Li-O_2 batteries by more than five times (from 20 to 106 cycles). It should be mentioned that besides the cathode side, the low charge voltage and the continuous lighting also weaken the corrosion of the Li anode, making the photo-assisted charging technology is beneficial to the whole Li-O_2 battery system.

2 Experimental

2.1 Materials

Tetraethylene glycol dimethyl ether (TEGDME, 99%), lithium bis((trifluoromethyl)sulfonyl)a-zanide (LiTFSI, 98%), dicyandiamide (98%), and cobalt(II) acetate (98%) were purchased from Aladdin Reagent. Lithium metal was obtained from China Energy Lithium Co., Ltd. CP was bought from Torray Japan. Dimethyl sulfoxide (DMSO)-d6 was purchased from Cambridge Isotope Laboratories.

2.2 Preparation of C_3N_4@CP and Co-C_3N_4@CP

1 mmol cobalt(II) acetate and 10 mmol dicyandiamide were thoroughly mixed and ground to get the precursor for preparing the Co-C_3N_4. Then, the precursor was dispersed in the mixed solvent of ethanol and Nafion solution and sprayed to a CP. After this, the precursor loaded CP was heated to 550 °C at a heating rate of 5 °C·min^{-1} in a tube furnace with an argon atmosphere for 4 h to obtain the Co-C_3N_4@CP. When cooling down, the Co-C_3N_4@CP was washed with water and ethanol three times to remove the unreacted residue, respectively. A similar method was used to prepare the C_3N_4@CP without adding cobalt(II) acetate. The mass loading of C_3N_4 or Co-C_3N_4 was 0.2–0.3 mg·cm^{-2}.

2.3 Cell assembly and electrochemical measurement

EL-cell type batteries (Fig. S7 in the Electronic Supplementary Material (ESM)) were assembled with C_3N_4@CP or Co-C_3N_4@CP as cathode, 1 M LiTFSI in TEGDME as electrolyte, and lithium sheet as anode to conduct the electrochemical measurement. The cathode shell was cut into a circular hole with a diameter of 10 mm to facilitate illumination. After assembling, the cell was placed in a photochemical reaction tank to ensure sufficient illumination of the photoelectrode. The Xe lamp with a power of 400 W was used as a light source, and the light intensity was controlled at 100 mW·cm^{-2}. Galva-nostatic discharge–charge and cycle life measurements were performed on a LAND (CT2100A) multi-channel battery testing system. Electrochemical impedance spectra (EIS), Mott–Schottky plots (test method in the ESM), and photocurrents tests were carried out on a Biologic VMP3 electrochemical station. The content of Li_2O_2 after discharge and charge of Li-O_2 cells with and without illumination was quantified by iodometry (test method in the ESM).

2.4 Characterization

Powder X-ray diffraction (XRD) measurement was carried out on a Bruker D8 powder X-ray diffractometer. Scanning electron microscopy (SEM) test was performed with a Hitachi S4800 field-emission scanning electron microscope. Fourier transform infrared (FTIR) spectroscopy characterization was examined by a Nicolet 6700 spectrometer. X-ray photoelectron spectroscopy (XPS) data was collected on a ThermoFisher ESCALAB MK II. Nuclear magnetic resonance (NMR) spectra were obtained on a Bruker Avance III 400 MHz instrument. Dimethyl sulfoxide-d6 was used as the inner standard solvent for hydrogen and carbon NMR measurement. Photoluminescence (PL) emission spectra were examined by a RERU-YQ-007 steady state and time-resolved fluorescence spectrometer.

3 Results and discussion

The Co-C_3N_4 was *in situ* fabricated on the CP via thermal evaporation of the dicyandiamide and cobaltous acetate mixture. The morphologies of CP, Co-C_3N_4@CP, and C_3N_4@CP are shown in Figs. 1(a) and 1(b), and Fig S1 in the ESM, respectively. It is clear that the CP is composed of carbon fibers with clean surfaces and diameters of approximately 10 μm (Fig. 1(a)), making it serve as a host for loading C_3N_4 or Co-C_3N_4 and a skeleton for fast electron transfer. For Co-C_3N_4, it grows on the fiber surfaces of CP with a morphology of layered flake aggregation (Fig. 1(b)). The element mappings (Fig. 1(c)) reveal the uniform distribution of Co, N, and C elements on the carbon fiber, indicating the successful preparation of Co-C_3N_4. In addition, energy dispersive X-ray spectroscopy (EDS) elemental analysis was also performed and confirmed the introduction of Co doping into the C_3N_4 (Fig. S2 in the ESM).

To illustrate the impact of Co doping on C_3N_4, characterizations like XRD, FTIR, and XPS were carried out. Figure 2(a) gives the crystalline structures of C_3N_4 and Co-C_3N_4. There are two typical peaks located at 13.3° and 27.5° corresponding to the in-planar repeated tri-s-triazine units of the (100) plane and the graphitic-like layered carbon nitride interlayer stack of the (002) plane of C_3N_4, respectively [30]. When introducing Co doping, the peak intensity at 13.3° weakens, which can be attributed to the fact that Co enters into the C_3N_4 planar structure and destroys its in-planar repeated tri-s-triazine units. Different from the (100) plane, the peak intensity for the (002) plane is enhanced, which is probably due to the slight increase of the interlayer spacing caused by the intercalated Co [31].

Figure 2(b) shows the FTIR spectra of C_3N_4 and Co-C_3N_4. It can be found that the Co doping does not change the location of absorption peaks of C_3N_4 except with slightly reduced peak intensity. The peaks at 809, 1,243, and the region of 1,400 to 1,650 cm^{-1} are related to the out of plane bending vibration mode of the triazine ring units, the stretching vibration of the C–N–C and C–NH–C, and the stretching vibration of the g-C_3N_4 heterocyclic ring, respectively. The chemical states of C, N, and Co elements in C_3N_4 and Co-C_3N_4 were verified by XPS spectra. As displayed in the C 1s spectra (Fig. 2(c)), the peaks of C_3N_4 at 288.8, 288.3, and 284.6 eV represent the C–N–C, N=C–C (C_3N_4), and C=C (CP), respectively. For the N 1s spectrum of C_3N_4 (Fig. 2(d)), it has three typical N peaks at 398.7 (C–N=C), 401.7 (C–N–H), and 396.5 eV (graphene N). When introducing Co doping, the C and N spectra of Co-C_3N_4 are consistent with the C_3N_4, while the Co spectrum shows clear Co 2p peaks (Fig. 2(e)), suggesting the successful doping of Co into the C_3N_4, and is consistent with the above results.

Since the electrons with absorbed energy would transit into the conduction band (CB) and then recombine with the remaining

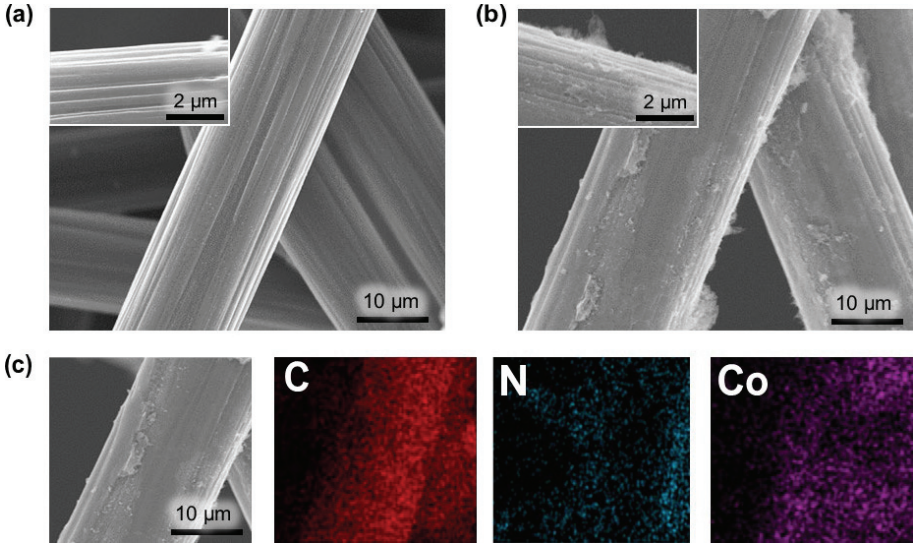

Figure 1 SEM images of the (a) CP and (b) Co-C_3N_4@CP. Insets are corresponding zoom-in images. (c) Element mappings of the Co-C_3N_4@CP cathode.

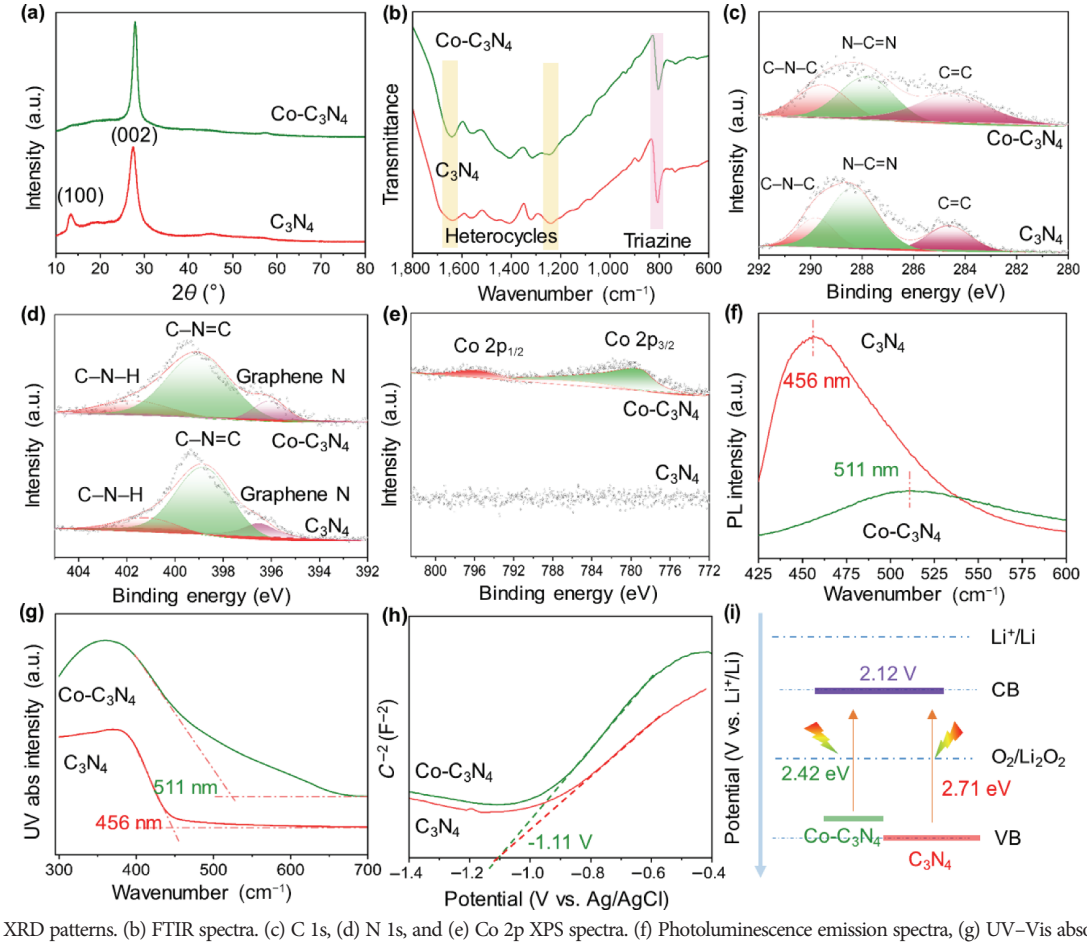

Figure 2 (a) XRD patterns. (b) FTIR spectra. (c) C 1s, (d) N 1s, and (e) Co 2p XPS spectra. (f) Photoluminescence emission spectra, (g) UV–Vis absorption spectra, (h) Mott–Schottky plot, and (i) potential diagram of CB and VB vs. Li^+/Li of the C_3N_4@CP and Co-C_3N_4@CP.

holes in the valence band (VB) to lead to PL [32], the band gaps [33] of C_3N_4 and Co-C_3N_4 were checked by the PL emission spectra (Fig. 2(f)). The PL intensity of C_3N_4 is much higher than that of Co-C_3N_4, indicating that the electrons and holes in C_3N_4 are more prone to recombine, and thus resulting in decreased available electrons and holes. In addition, compared to C_3N_4, the peak from Co-C_3N_4 exhibits a red shift from 456 to 511 nm, revealing that the band gap (calculation method in the ESM) is narrowed from 2.71 (C_3N_4) to 2.42 eV (Co-C_3N_4) by Co doping. This would broaden the range of photo response and enhance the photocatalytic ability of Co-C_3N_4. The Co doping induced photo response performance enhancement of C_3N_4 can be further demonstrated by the ultraviolet–visible (UV–Vis) absorption spectra (Fig. 2(g)). Moreover, the photocurrent density of Co-C_3N_4 is twice that of C_3N_4 (Fig. S3 in the ESM), indicating that the Co-C_3N_4 has better photo response and higher charge transfer rate, which is consistent with the PL and UV–Vis analysis results. To determine the CB potential of the C_3N_4 and Co-C_3N_4, Mott–Schottky plots were used to test the flat band potential [22]. Both C_3N_4 and Co-C_3N_4 possess the same flat band potential of −1.11 V vs. AgCl/Ag (Fig. 2(h)). Then, the CB and VB potentials of C_3N_4 and Co-C_3N_4 can be calculated and together with the theoretical decomposition potential of Li_2O_2 are listed in Fig. 2(i). It can be seen that the VB potential of Co-C_3N_4 is lower than that

of C_3N_4, but both of them are higher than the theoretical decomposition potential of Li_2O_2, making the photo-generated holes of C_3N_4 and Co-C_3N_4 have the ability to facilitate the oxidization of Li_2O_2.

After confirming the theoretical feasibility of C_3N_4 and Co-C_3N_4 in promoting the decomposition of Li_2O_2 through photo-assisted charging technology, their practical applicability in Li-O_2 batteries was checked. Figure 3(a) displays the charge/discharge curves of the C_3N_4 and Co-C_3N_4 at 500 mAh·g^{-1} and 100 mA·g^{-1}. It points out that the Co doping could significantly reduce the charge and discharge overpotentials of Li-O_2 batteries even without illumination, which is attributed to the Co doping rendered increased conductivity and oxygen reduction reaction (ORR) and OER catalytic ability of C_3N_4. When introducing illumination, the median charge voltages for C_3N_4 and Co-C_3N_4 decrease from 3.95 to 3.36 V and 3.90 to 3.30 V at 500 mAh·g^{-1} and 100 mA·g^{-1} (Fig. 3(b) and Fig. S4 in the ESM), respectively, which is consistent with the lower VB potential of Co-C_3N_4 than that of C_3N_4. Benefiting from the low overpotential brought by the Co-C_3N_4 without illumination, the cycle life of the battery with Co-C_3N_4 is more than five times to that of the one with C_3N_4 at 100 mA·g^{-1} (106 cycles vs. 20 cycles, Fig. 3(c)). While under illumination, the Co-C_3N_4 based battery could sustain a low charge voltage of below 3.5 V at 200 mA·g^{-1} for more than 300 h (Fig. 3(d)), much better than the battery without illumination that has large polarization potentials and short cycle life of approximately 150 h. This significant performance improvement can be attributed to the fully functioned photocatalytic ability of Co-C_3N_4 that promotes the decomposition of Li_2O_2 at low charge overpotentials with reduced side reactions and decreased battery impedance (Fig. S5 in the ESM).

To demonstrate that the photo-generated holes could indeed decompose the Li_2O_2, the composition and morphology evolution of Co-C_3N_4@CP cathodes at different cycles under illumination were detected by XRD, SEM, and FTIR. The XRD patterns in Fig. 4(a) show that two new peaks at 32.8° and 34.8° corresponding to the Li_2O_2 emerge in the discharged cathode, and these two peaks disappear after the subsequent charge process, revealing that the

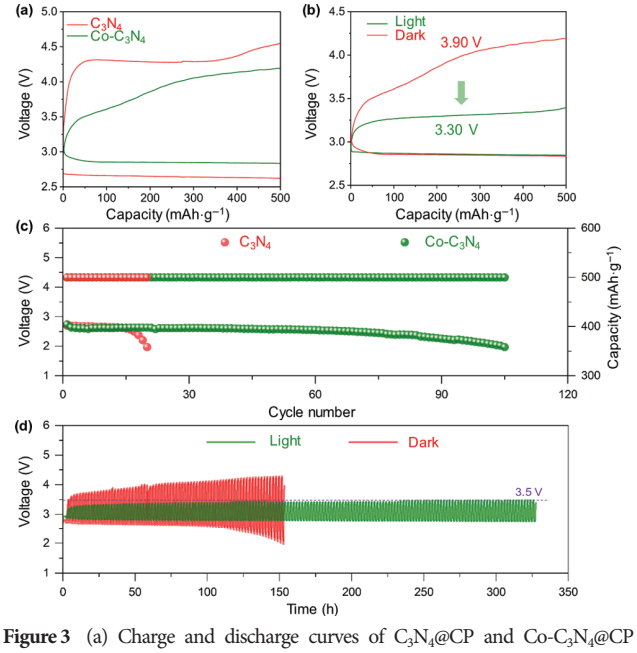

Figure 3 (a) Charge and discharge curves of C_3N_4@CP and Co-C_3N_4@CP without illumination at 100 mA·g^{-1}. (b) Charge and discharge curves of Co-C_3N_4@CP with and without illumination at 100 mA·g^{-1}. (c) Cycle performance of Li-O_2 batteries using C_3N_4@CP and Co-C_3N_4@CP cathodes without illumination at 100 mA·g^{-1}. (d) Cycle performance of Li-O_2 batteries using Co-C_3N_4@CP cathodes with and without illumination at 200 mA·g^{-1}.

photo-assisted Li-O_2 battery follows the conventional Li-O_2 battery electrochemistry with the formation and decomposition of Li_2O_2. It should be mentioned that even after 30 cycles, there are still no peaks from residual Li_2O_2 or any other by-products, indicating that the photo-generated holes could decompose Li_2O_2 at lower overpotentials and inhibit the occurrence of side reactions. To further confirm this, the Li_2O_2 contents of the photo-assisted Li-O_2 batteries after discharge and charge were quantitatively analyzed by iodometry (Table S1 in the ESM) [34]. The battery with illumination delivers a Li_2O_2 yield of 85.4%, which is a little bit higher than that without illumination (84.7%). When charging to 4 V, the Li_2O_2 of the photo-assisted Li-O_2 battery could be completely decomposed, while there is still some remnant Li_2O_2 for the one without illumination. The FTIR spectra also confirm this result. Different from the clear LiOH peak for the discharged cathode without illumination, no LiOH but only Li_2O_2 can be detected on the discharged cathode with illumination (Fig. 4(b)), which can be ascribed to the photo-assisted low charge voltage without inducing the formation of H_2O from electrolyte decomposition. The morphologies of the Co-C_3N_4@CP cathodes at discharge and charge states are shown in Figs. 4(c) and 4(d). It can be seen that just like the cathode without illumination (Fig. S6 in the ESM), toroidal-type Li_2O_2 disperses on the Co-C_3N_4@CP with illumination (Fig. 4(c)), and the discharge product disappears after charging, suggesting the high reversibility of the Li_2O_2. To further illustrate the photocatalytic decomposition of Li_2O_2, the gas evolution during the charge process was monitored by differential electrochemical mass spectrometry (DEMS) using an EL cell (Fig. S7 in the ESM). From Figs. 4(e) and 4(f) we can see that the photo-assisted charging enables more oxygen release than traditional charging at the early stage, signifying the photocatalytic decomposition of Li_2O_2 at low overpotentials. To compare the released O_2 in the two cases, we have calculated the integrated areas of the O_2 evolution curves in Figs. 4(e) and 4(f). The photo-assisted Li-O_2 battery has an area of 2.017, while the area for conventional Li-O_2 battery is only 1.876 (Fig. S8 in the ESM). So the illuminated case released more O_2 than the dark one, thus a high reversibility for the cell with illumination. In addition, XRD patterns and SEM images of the discharge cathodes with different illumination times are shown in Figs. S9 and S10 in the ESM. As the illumination time increases, the intensity of Li_2O_2 peak gradually weakens, and the morphology of Li_2O_2 changes from perfect to shriveled and cracked toroidal, again signifying the photocatalytic decomposition of Li_2O_2 at low overpotentials. The above analysis certifies that the designed Co-C_3N_4 could behave as an efficient photocatalyst to facilitate the decomposition of Li_2O_2 at low overpotentials to improve the energy efficiency and lifetime of Li-O_2 batteries.

Since we have known the advantages brought by the photo-assisted charging technology on the cathode side, whether there will be any beneficial or harmful effect on the Li anode and electrolyte with illumination? To answer this question, the status of the Li anode and electrolyte with illumination was characterized. Figures 5(a) and 5(b) show the morphology of the 1st cycled Li anodes. Compared with the Li anode without illumination (Fig. 5(a)), the one with illumination exhibits a much smoother surface with fewer cracks (Fig. 5(b)). Then, XRD was performed to check the composition change of the Li anodes sealed in the device in Fig. S11 in the ESM. Unlike the obvious LiOH peaks for the Li anodes after the 1st and 5th cycles without illumination (Fig. S12 in the ESM), the introduction of illumination could reduce the LiOH content on the Li anode. This is because the limited water generation due to the low charge overpotential suppresses the decomposition of the electrolyte. To illustrate the stability of the electrolyte under illumination, the

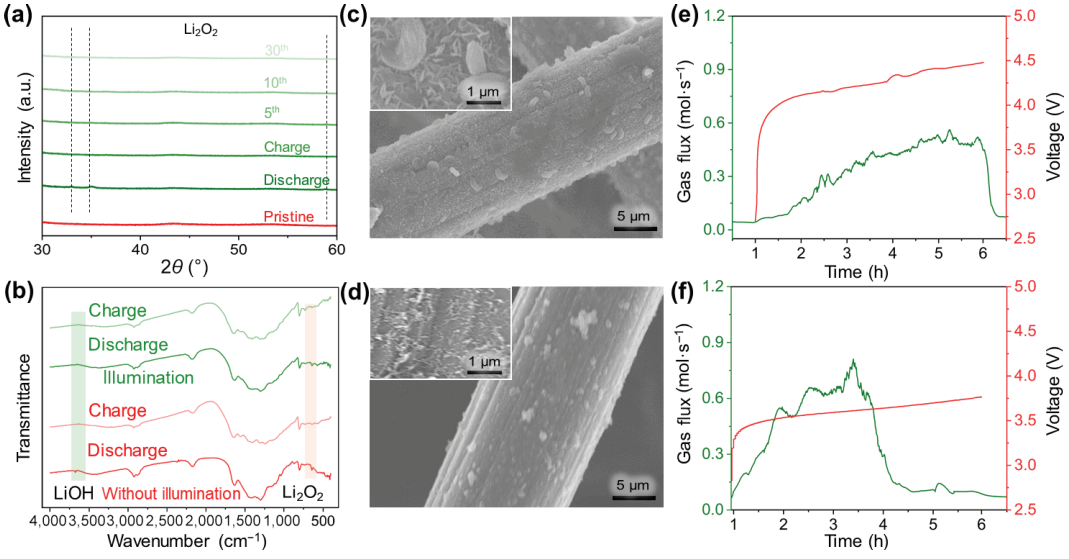

Figure 4 (a) XRD patterns of the Co-C_3N_4 cathodes after different cycles. (b) FTIR spectra of the Co-C_3N_4 cathodes with and without illumination. ((c) and (d)) SEM images of the Co-C_3N_4 cathodes at (c) discharge and (d) charge states with illumination. ((e) and (f)) DEMS test for the charge process of the Li-O_2 batteries after being discharged to 0.5 mAh (e) without and (f) with illumination.

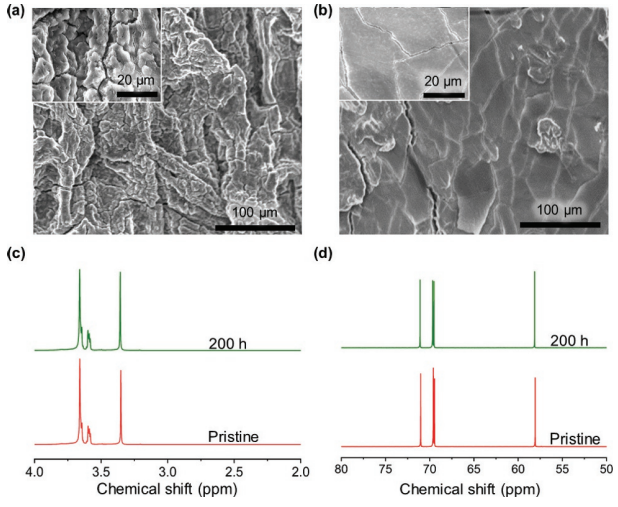

Figure 5 SEM images of the Li anodes after the first cycle (a) without illumination and (b) with illumination. (c) Hydrogen and (d) carbon NMR spectra of the electrolyte under different illumination times.

NMR spectra of hydrogen and carbon were detected. There are no new peaks in both spectra after 200 h of illumination (Figs. 5(c) and 5(d)), demonstrating that the electrolyte could sustain a long time of illumination without decomposition. These results well answer the above question that the introduction of illumination has a positive effect on the Li anode and almost no effect on the electrolyte.

4 Conclusions

In summary, a new Co doped C_3N_4 photocatalyst was *in situ* grown on the carbon paper via a thermal evaporation method to behave as the photo and oxygen cathode for Li-O_2 batteries. The Co doping can not only enhance the electrical conductivity and photoresponse ability of C_3N_4, but also improve its ORR and OER catalytic properties. Thanks to these benefits, even without illumination, the Co-C_3N_4 could significantly reduce the overpotential and prolong the lifetime (from 20 to 106 cycles) of Li-O_2 batteries. While introducing illumination, the Co doping accelerates the separation of photo-generated electrons and holes, and accordingly improves the photocatalytic ability of C_3N_4, which further reduces the charge overpotential from 3.90 to 3.30 V and enables the battery to maintain low charge voltages of below 3.5 V exceeding 300 h. Moreover, the photo-assisted low charge overpotential limits the high voltage associated side reactions, like electrolyte decomposition, and thus alleviates the corrosion of Li anode. Therefore, the Co-C_3N_4 takes advantage of the photo-assisted charging technology could to some extent conquer the high charge overpotential and Li anode corrosion issues of Li-O_2 batteries, bringing Li-O_2 batteries one step closer to being viable energy storage devices.

Acknowledgements

The authors thank the supports from the National Key Research and Development (R&D) Program of China (No. 2017YFE0198100), the National Natural Science Foundation of China (No. 21725103), Key Research Program of the Chinese Academy of Sciences (No. ZDRW-CN-2021-3), Youth Innovation Promotion Association of Chinese Academy of Sciences (No. 2020230), and Changchun Science and Technology Development Plan Funding Project (No. 21ZY06).

Electronic Supplementary Material: Supplementary material (the test method of Mott–Schottky plots, quantification of Li_2O_2 by iodometry and calculating the band gap, SEM, EDS, photocurrent density, impedance, EL-cell, and XRD) is available in the online version of this article at https://doi.org/10.1007/s12274-022-5300-8.

References

[1] Liu, T.; Vivek, J. P.; Zhao, E. W.; Lei, J.; Garcia-Araez, N.; Grey, C. P. Current challenges and routes forward for nonaqueous lithium-air batteries. *Chem. Rev.* **2020**, *120*, 6558–6625.

[2] Gao, X. W.; Chen, Y. H.; Johnson, L. R.; Jovanov, Z. P.; Bruce, P. G. A rechargeable lithium-oxygen battery with dual mediators stabilizing the carbon cathode. *Nat. Energy* **2017**, *2*, 17118.

[3] Johnson, L.; Li, C. M.; Liu, Z.; Chen, Y. H.; Freunberger, S. A.; Ashok, P. C.; Praveen, B. B.; Dholakia, K.; Tarascon, J. M.; Bruce, P. G. The role of LiO_2 solubility in O_2 reduction in aprotic solvents and its consequences for Li-O_2 batteries. *Nat. Chem.* **2014**, *6*, 1091–1099.

[4] Shen, Z. Z.; Zhou, C.; Wen, R.; Wan, L. J. Charge rate-dependent decomposition mechanism of toroidal Li_2O_2 in Li-O_2 batteries. *Chin. J. Chem.* **2021**, *39*, 2668–2672.

[5] Peng, X. H.; Wang, C.; Liu, Y. H.; Fang, W. W.; Zhou, Y. S.; Fu, L.

J.; Ye, J. L.; Liu, L. L.; Wu, Y. P. Critical advances in re-engineering the cathode-electrolyte interface in alkali metal-oxygen batteries. *Energy Mater* **2021**, *1*, 100011.

[6] Yao, W. T.; Yuan, Y. F.; Tan, G. Q.; Liu, C.; Cheng, M.; Yurkiv, V.; Bi, X. X.; Long, F.; Friedrich, C. R.; Mashayek, F. et al. Tuning Li_2O_2 formation routes by facet engineering of MnO_2 cathode catalysts. *J. Am. Chem. Soc.* **2019**, *141*, 12832–12838.

[7] Xu, J. J.; Wang, Z. L.; Xu, D.; Zhang, L. L.; Zhang, X. B. Tailoring deposition and morphology of discharge products towards high-rate and long-life lithium-oxygen batteries. *Nat. Commun.* **2013**, *4*, 2438.

[8] Wang, J. W.; Ma, L. P.; Xu, J. Y.; Xu, Y.; Su, K.; Peng, Z. Q. Oxygen electrochemistry in Li-O_2 batteries probed by *in situ* surface-enhanced Raman spectroscopy. *SusMat* **2021**, *1*, 345–358.

[9] Kwak, W. J.; Rosy; Sharon, D.; Xia, C.; Kim, H.; Johnson, L. R.; Bruce, P. G.; Nazar, L. F.; Sun, Y. K.; Frimer, A. A. et al. Lithium-oxygen batteries and related systems: Potential, status, and future. *Chem. Rev.* **2020**, *120*, 6626–6683.

[10] Wang, Y.; Lai, N. C.; Lu, Y. R.; Zhou, Y. C.; Dong, C. L.; Lu, Y. C. A solvent-controlled oxidation mechanism of Li_2O_2 in lithium-oxygen batteries. *Joule* **2018**, *2*, 2364–2380.

[11] Song, L. N.; Zhang, W.; Wang, Y.; Ge, X.; Zou, L. C.; Wang, H. F.; Wang, X. X.; Liu, Q. C.; Li, F.; Xu, J. J. Tuning lithium-peroxide formation and decomposition routes with single-atom catalysts for lithium-oxygen batteries. *Nat. Commun.* **2020**, *11*, 2191.

[12] Wang, P.; Ren, Y. Y.; Wang, R. T.; Zhang, P.; Ding, M. J.; Li, C. X.; Zhao, D. Y.; Qian, Z.; Zhang, Z. W.; Zhang, L. Y. et al. Atomically dispersed cobalt catalyst anchored on nitrogen-doped carbon nanosheets for lithium-oxygen batteries. *Nat. Commun.* **2020**, *11*, 2811.

[13] Gu, T. H.; Agyeman, D. A.; Shin, S. J.; Jin, X. Y.; Lee, J. M.; Kim, H.; Kang, Y. M.; Hwang, S. J. α-MnO_2 nanowire-anchored highly oxidized cluster as a catalyst for Li-O_2 batteries:Superior electrocatalytic activity and high functionality. *Angew. Chem., Int. Ed.* **2018**, *57*, 15984–15989.

[14] Gao, X. W.; Jovanov, Z. P.; Chen, Y. H.; Johnson, L. R.; Bruce, P. G. Phenol-catalyzed discharge in the aprotic lithium-oxygen battery. *Angew. Chem., Int. Ed.* **2017**, *56*, 6539–6543.

[15] Liu, T.; Liu, Z. G.; Kim, G.; Frith, J. T.; Garcia-Araez, N.; Grey, C. P. Understanding LiOH chemistry in a ruthenium-catalyzed Li-O_2 battery. *Angew. Chem., Int. Ed.* **2017**, *56*, 16057–16062.

[16] Lu, J.; Lee, Y. J.; Luo, X. Y.; Lau, K. C.; Asadi, M.; Wang, H. H.; Brombosz, S.; Wen, J. G.; Zhai, D. Y.; Chen, Z. H. et al. A lithium-oxygen battery based on lithium superoxide. *Nature* **2016**, *529*, 377–382.

[17] Peng, Z. Q.; Freunberger, S. A.; Chen, Y. H.; Bruce, P. G. A reversible and higher-rate Li-O_2 battery. *Science* **2012**, *337*, 563–566.

[18] Liang, J. S.; Xia, Y.; Liu, X.; Huang, F. Y.; Liu, J. J.; Li, S. Z.; Wang, T. Y.; Jiao, S. H.; Cao, R. G.; Han, J. T. et al. Molybdenum-doped ordered $L1_0$-PdZn nanosheets for enhanced oxygen reduction electrocatalysis. *SusMat* **2022**, *2*, 347–356.

[19] Xia, Q.; Zhai, Y. J.; Zhao, L. L.; Wang, J.; Li, D, Y.; Zhang, L. L.; Zhang, J. T. Carbon-supported single-atom catalysts for advanced rechargeable metal-air batteries. *Energy Mater* **2022**, *2*, 200015.

[20] Gao, X. W.; Chen, Y. H.; Johnson, L.; Bruce, P. G. Promoting solution phase discharge in Li-O_2 batteries containing weakly solvating electrolyte solutions. *Nat. Mater.* **2016**, *15*, 882–888.

[21] Lin, X. D.; Yuan, R. M.; Cao, Y.; Ding, X. B.; Cai, S. R.; Han, B. W.; Hong, Y. H.; Zhou, Z. Y.; Yang, X. L.; Gong, L.; et al. Controlling reversible expansion of Li_2O_2 formation and decomposition by modifying electrolyte in Li-O_2 batteries. *Chem* **2018**, *4*, 2685–2698.

[22] Li, M. L.; Wang, X. X.; Li, F.; Zheng, L. J.; Xu, J. J.; Yu, J. H. A bifunctional photo-assisted Li-O_2 battery based on a hierarchical heterostructured cathode. *Adv. Mater.* **2020**, *32*, 1907098.

[23] Lee, S. H.; Park, J. B.; Lim, H. S.; Sun, Y. K. An advanced separator for Li-O_2 batteries: Maximizing the effect of redox mediators. *Adv. Energy Mater.* **2017**, *7*, 1602417.

[24] Sun, H. W.; Quan, F. J.; Mao, C. L.; Zhang, L. Z. New strategies for nitrogen fixation and pollution control. *Chin. J. Chem.* **2021**, *39*, 3199–3210.

[25] Zhang, G.; Liu, B.; Wang, T.; Gong, J. L. Arificial leaves for solar fuels. *Chin. J. Chem.* **2021**, *39*, 1450–1458.

[26] Kim, J. H.; Constantin, T.; Simonetti, M.; Llaveria, J.; Sheikh, N. S.; Leonori, D. A radical approach for the selective C-H borylation of azines. *Nature* **2021**, *595*, 677–683.

[27] Yu, M. Z.; Ren, X. D.; Ma, L.; Wu, Y. Y. Integrating a redox-coupled dye-sensitized photoelectrode into a lithium-oxygen battery for photoassisted charging. *Nat. Commun.* **2014**, *5*, 5111.

[28] Zhu, Z.; Shi, X. M.; Fan, G. L.; Li, F. J.; Chen, J. Photo-energy conversion and storage in an aprotic Li-O_2 battery. *Angew. Chem., Int. Ed.* **2019**, *58*, 19021–19026.

[29] Yang, X. Y.; Feng, X. L.; Jin, X.; Shao, M. Z.; Yan, B. L.; Yan, J. M.; Zhang, Y.; Zhang, X. B. An illumination-assisted flexible self-powered energy system based on a Li-O_2 battery. *Angew. Chem., Int. Ed.* **2019**, *58*, 16411–16415.

[30] Liu, J.; Liu, Y.; Liu, N. Y.; Han, Y. Z.; Zhang, X.; Huang, H.; Lifshitz, Y.; Lee, S. T.; Zhong, J.; Kang, Z. H. Metal-free efficient photocatalyst for stable visible water splitting via a two-electron pathway. *Science* **2015**, *347*, 970–974.

[31] Li, M.; Qi, T. Y.; Yang, R. X.; Xiao, H. N.; Fang, Z. M.; Hodge, S. A.; James, T. D.; Wang, L. D.; Mao, B. Y. Promoting magnesium sulfite oxidation via partly oxidized metal nanoparticles on graphitic carbon nitride (g-C_3N_4) in the magnesia desulfurization process. *J. Mater. Chem. A* **2018**, *6*, 11296–11305.

[32] Yu, Y.; Yan, W.; Wang, X. F.; Li, P.; Gao, W. Y.; Zou, H. H.; Wu, S. M.; Ding, K. J. Surface engineering for extremely enhanced charge separation and photocatalytic hydrogen evolution on g-C_3N_4. *Adv. Mater.* **2018**, *30*, 1705060.

[33] Kudo, A.; Miseki, Y. Heterogeneous photocatalyst materials for water splitting. *Chem. Soc. Rev.* **2009**, *38*, 253–278.

[34] Kundu, D.; Black, R.; Adams, B.; Nazar, L. F. A highly active low voltage redox mediator for enhanced rechargeability of lithium-oxygen batteries. *ACS Cent. Sci.* **2015**, *1*, 510–515.